chapter five

PLASMA CHARACTERISTICS FROM PROBE AND SPECTRAL EMISSION MEASUREMENTS

5.1 Langmuir probe measurements

Within the limitations and sensitivity of the present Langmuir probe diagnostic setup discussed in *Section 3.3*, the range of operating conditions of the hollow cathode discharge for which the probe characteristics can be obtained are (*2, 6, 12* and *20)mbar* at (*5, 10, 20* and *40)mA* for the HC6512 and (*6* and *12)mbar* at (*5, 10, 20* and *40)mA* for the HC1612. For comparison purposes, the smallest(*0.65cm*) and largest(*1.6cm*) diameter hollow cathodes are investigated. The limitation and sensitivity problems encountered are:

(a) peak-to-peak probe current $i_P(t)$ which is larger than *10%* of the discharge current i_A that can cause serious disturbances to the discharge,

(b) $i_P(t)$ which is too small to be doubly differentiated properly (even with postfilter gain of *20dB*),

(c) the required bias voltage to the probe V_A is larger than the maximum(*~600V*) available from the battery pack (this is especially so at $p=0.5mbar$ as its sustaining voltage is high), and

(d) the presence of some stubborn noise distortion to probe voltage and current signals(at frequencies lower than the set cutoff frequency of the low-pass filter).

Despite these problems, probe characteristics for hollow cathode discharges similar to those discussed in *Section 4.2.1* have been obtained. The measurements are made at the middle cross-sectional plane of only the shorter hollow cathode of *1.2cm* (l_K:a being *1.85* and *0.75* for HC6512 and HC1612 respectively). It is assumed to have reasonably axial homogeneity here since *Mizeraczyk*[MIZ87] has shown that axial inhomogeneity (in terms of the electron energy distribution function, mean energy and concentration of electrons, and plasma potential) gets more pronounced when l_K:a is larger than *3.1* in a *stainless steel* hollow cathode of inner diameter *0.5cm* operated in helium. The pressure also affects the axial homogeneity; high pressure is preferred as shown by *Borodin et al.*[BOR67b] and *Mizeraczyk*[MIZ87] in their respective hollow cathode discharge systems. The radial homogeneity of the present hollow cathode discharge is investigated by comparing the plasma parameters deduced from the probe characteristics at the axis and at a distance d_P (*0.2cm* for HC6512 and *0.4cm* for HC1612) off-axis. The signals of $i_P(t)$ and $V_P(t)$ are then digitally processed according to the procedure outlined in *Section 3.3.2* with a fitting width of m=*70* and subsequently, some of the plasma parameters of the hollow cathode discharge are deduced.

5.1.1 The electron temperature and its density

In assuming a collisionless plasma (of which its validity over the operating conditions has been discussed in *Section 3.3*), the electron temperature T_e is deduced from the slope of the electron retardation region of the plot of $ln(I_e)$ against V_p according to equation (*3.3.2*). The plasma potential is estimated at the point of intersection between the extrapolated linear lines of the electron retardation region and the electron saturation region of the same plot. The electron density, in turn, is estimated from equation (*3.3.3*) with a known effective probe surface area $A_p = 4.91\times10^{-8}\ m^2$.

In cases where two distinct linear regions are observable on the electron retardation region as shown in *Figure 5.1.1*, it shall be interpreted as evidence of the existence of two groups of electrons with Maxwellian distributions at different temperatures (assuming that the effect due to a change in the contact potential between the probe and the plasma has been minimized as discussed in *Section 3.3.1*). The existence of more than one group of electrons in hollow cathode discharge has been investigated by various workers as discussed in *Section 2.3*. In this case, the procedure used by *Tkachenko and Tyutyunnik*[TKA76] shall be adopted to evaluate the temperatures and densities of the two groups of electrons. The temperature of the 'fast' group T_f is determined from the slope of the lower linear part of the characteristic. This line is extrapolated to the plasma potential to deduce its saturation current in order to evaluate the density of this group of electrons n_f. To determine the temperature of the 'slow' group of electrons, the current due to the 'fast' electrons is subtracted from the total electron current for each corresponding

probe potential. The slope of the straight line of the subtracted current will then be used to determine the temperature of the 'slow' electrons T_s. The difference between the total electron current and the current due to the 'fast' electrons at the plasma potential can be taken to be the saturation current of the 'slow' electron group; from which its density n_s is then deduced. The average energy T_e and the total electron density n_e are calculated according to:

$$(n_s + n_f)T_e = n_s T_s + n_f T_f \quad , \qquad (5.1.1)$$

and

$$n_e = n_s + n_f \quad . \qquad (5.1.2)$$

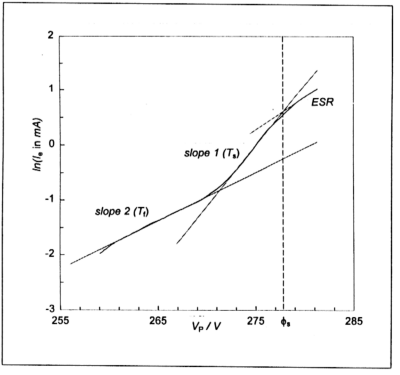

Figure 5.1.1 Plot of $ln(I_e)$ against V_P at *6mbar, 40mA* in the HC6512 (axis) exhibiting two linear portions in the electron retardation region. T_f is deduced from *slope 2* and T_s from *slope 1*. *ESR* refers to the electron saturation region.

The average electron energy T_e and the total electron density n_e deduced according to the procedure outlined above are shown in *Figures 5.1.2(a)-(d)* in

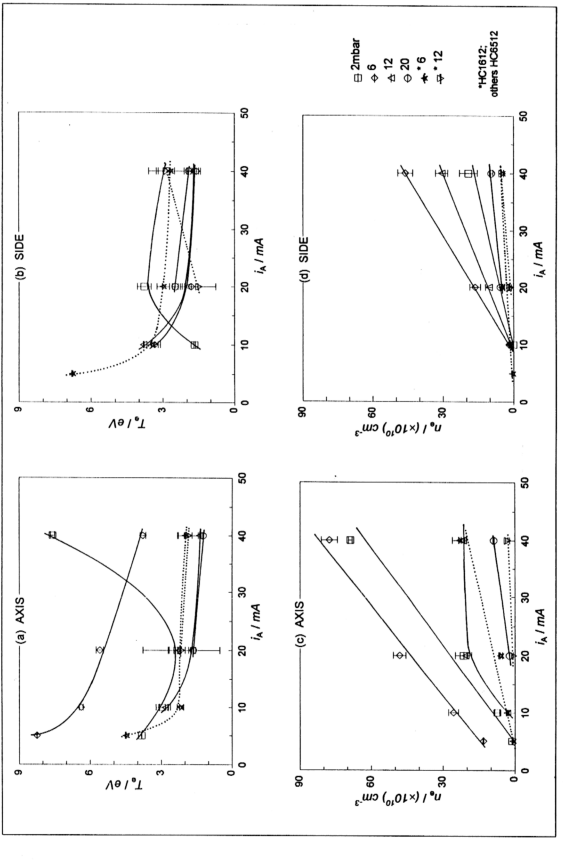

Figure 5.1.2 Dependence of T_e and n_e on i_A at various fixed *He* pressures monitored at the axes and sides of the hollow cathodes HC6512 and HC1612.

relation to the discharge current i_A at various fixed *He* pressure p. T_e(at the axis and side positions) generally decreases with increasing i_A, the fall being steep initially and getting more gradual at higher i_A. A distinctive exception is observed with the HC6512 at *2mbar* equivalent to *ap=0.975cm-torr* which is just outside the lower limit of the applicability range of the hollow cathode discharge discussed in *Section 1.1*. T_e at the axis falls initially until *20mA*, after which it rises while the inverse is true for T_e at the side. The general behaviour of the variation of T_e with i_A is similar to those observed in an *Ar* hollow cathode discharge {diameter *2cm*; length *7.4cm* and a *He-Ni* hollow cathode discharge {diameter *3cm*; length *20cm*} by *Tkachenko and Tyutyunnik*[TKA76]. *Mizeraczyk*[MIZ87], however, showed that the T_e in a *He-stainless steel* hollow cathode discharge {diameter *0.5cm*; lengths *0.77cm* and *1.55cm*} falls initially with increasing i_A until approximately *(10-20)mA* before increasing very slowly with further increase of i_A. The n_e at the axis and side generally rise linearly with i_A (except for *12mbar*(HC6512), whereby n_e becomes quite constant at larger i_A); the slope being greater for smaller hollow cathode diameter a at fixed pressure p. Similar variation is also observed by *Howorka and Pahl*(except at *p=1torr* for which n_e is constant at low i_A) and *Mizeraczyk*. Increasing the discharge current results in increased rate of ionization and, therefore, the electron number density. This leads to lower electron temperature as the probability of an electron being able to attain high energy is reduced. This inference should be reflected in the behaviour of the ratio of the number densities of the 'fast' electrons to 'slow' ones, that is, n_f/n_s which is shown in *Figures 5.1.3(a)-(b)*. The ratio n_f/n_s decreases as i_A is increased for most of the conditions studied except for a few cases, namely at *12mbar*(axis) and *20mbar*(side) for HC6512 and *6mbar*(axis)

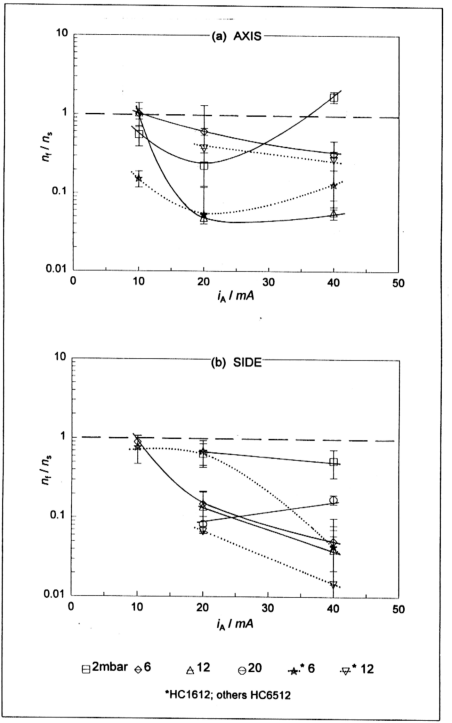

Figure 5.1.3 Variation of the ratio n_i/n_s with i_A at various fixed *He* pressures *p* monitored at the axes and sides of the hollow cathodes HC6512 and HC1612.

for HC1612, for which n_f/n_s increases slightly at the higher currents. However, these variations from the general behaviour may be ignored as they occur at pressures where the reliability of the probe is questionable (error expected to be > *25%*) as discussed in *Section 3.3*. The most prominent exception is again at *2mbar(axis)* for the HC6512 where at *40mA*, n_f/n_s increases to a value larger than unity. This exception is mirrorred in its electron energy distribution function whereby the *f(ε)* displays relatively high values at the high electron energy ε end (see *Section 5.1.2*) and it is also consistent with the earlier observation of its behaviour of T_e with i_A. Similar general behaviou of n_f/n_s with i_A has been shown by *Howorka and Pahl*(except at *p=1torr* again in which n_f/n_s peaks at *10mA*).

Similar trends are also observed for the T_e and n_e estimated from the second derivative of the probe characteristics d^2I_e/dV_p^2 where integrations according to equations *(3.3.7)* and *(3.3.8)* are carried out up to the limit of V when d^2I_e/dV_p^2 just approaches zero. Values of d^2I_e/dV_p^2 beyond this limit are doubtful as uncertainties in the digitized probe signals can be exaggerated. However, the magnitudes of T_e and n_e deduced through both the methods mentioned earlier are found to differ; by as much as *90%* for T_e and *60%* for n_e in some cases. In comparison, *Tkachenko and Tyutyunnik*[TKA76] have reported similar differences in the average energies of up to *40%* (only in the higher pressure range of *(0.5-2)torr*) while the densities can differ by as large as *20-25%*. These differences could be due to the assumed Maxwellian distribution in the deduction through the $ln(I_e)-V_p$ curves and the truncation error due to the discrete upper limit in the integration procedure when deduced through the d^2I_e/dV_p^2-V curves. The actual type of electron energy distribution function is determined from the $d^2I_e/dV_p^2 \cdot V^{1/2}-V$ curves and is discussed in *Section 5.1.2*.

The dependence of the estimated temperatures and densities of the 'slow' and 'fast' electrons, T_s, T_f, n_s and n_f, on the discharge current i_A at various fixed *He* pressures p are shown in *Figures 5.1.4(a)-(d)* and *5.1.5(a)-(d)*. The magnitudes of T_s and T_f fall within the ranges *(1-3)eV* and *(4-17)eV* respectively. Thus, the slow group belongs to the third group*(iii)* while the fast ones belong to the second group*(ii)* at the lower energy range described in *Section 2.3*. The 'fast' group of electrons here could be the ones responsible for the H_α *656.28nm* emission line observed in the hollow cathode discharge (see *Section 5.2.1*). However, most of the electrons capable of exciting and ionizing for the *He* hollow cathode discharge belong to the second group*(ii)* at the higher energy range of *(19-26)eV*[BOR66]. The presence of this electron group of interest would be evident from the electron energy distribution function which is discussed in *Section 5.1.2* and indirectly, from the observed radial distribution of the emission lines discussed in *Section 5.2.1*. The trend of the variation of T_s and T_f with i_A is dependent on the *He* pressure p. Anyhow, T_s(axis and side) decreases with increasing i_A for most of the p studied while T_f(axis) increases with i_A up to *20mA* before decreasing at most p and T_f(side) generally increases with i_A. The density of the slow electrons n_s (axis and side), however, can be said to generally increase quite linearly with i_A (except at *12mbar*(HC6512), whereby, n_s reaches saturation after *20mA*). The largest gradient is exhibited at *6mbar*(HC6512) while steeper gradient (at fixed p) is supported by the hollow cathode of smaller diameter. The density of the fast electrons n_f varies comparatively less with i_A except at *2mbar*(HC6512) for which n_f increases rather steeply with i_A. *Howorka and Pahl* reported correspondingly lower magnitudes at T_s=*(0.07-1.0)eV* and T_f=*(2.0-3.2)eV* but in a different hollow cathode discharge

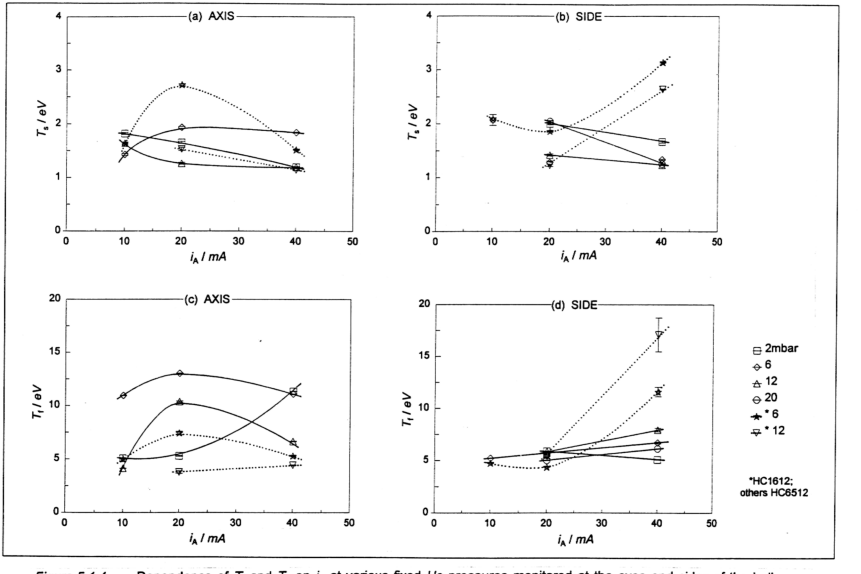

Figure 5.1.4 Dependence of T_f and T_s on i_A at various fixed *He* pressures monitored at the axes and sides of the hollow cathodes HC6512 and HC1612.

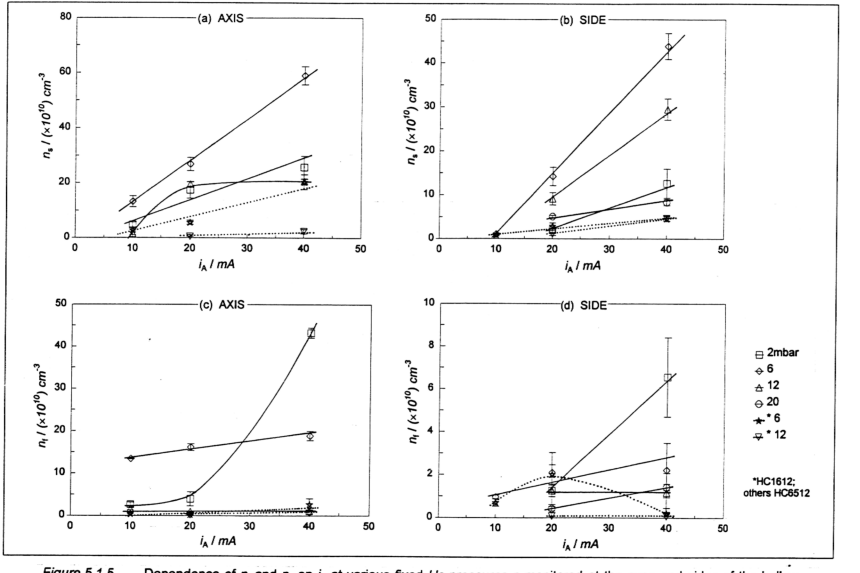

Figure 5.1.5 Dependence of n_f and n_s on i_A at various fixed *He* pressures *p* monitored at the axes and sides of the hollow cathodes HC6512 and HC1612.

system with smaller range of i_A from *5mA* to *20mA*. In their case, T_s decreases while T_f increases with increasing i_A though n_s and n_f are generally proportional to i_A. A comparison of the behaviour of the plasma parameters with i_A of the present system with those observed by other workers is summarized in *Table 5.1.1*.

It is also more appropriate to study the behaviour of the plasma parameters with respect to the product of the hollow cathode diameter and operating pressure *ap*(in *cm-torr*). It can then be related to the optimum pressure regime in which the hollow cathode discharge is said to be fully developed. As such, the dependence of the electron temperatures(T_e, T_s and T_f) and densities(n_e, n_s and n_f) at the axes and sides of both hollow cathodes HC6512 and HC1612 on *ap* are shown in *Figures 5.1.6(a)-(e)*. *Figure 5.1.6(f)* shows the corresponding variation of the discharge voltage V_A and plasma potential ϕ_S with *ap* at fixed discharge current i_A of *40mA*; from which the *optimum pressure range* is estimated at *(2-6)cm-torr* for the HC6512(the range estimated from the *V-i* curves in *Section 4.2.1* is at *(1-5)cm-torr*). Eventhough the same range could not be determined for the HC1612 due to insufficient data points, the range is expected to shift to slightly larger values of *ap* as has been shown in *Section 4.2.1*. The variation of the plasma potential ϕ_S follows that of the sustaining voltage of the discharge V_A except that it is at lower magnitude. The difference in magnitude ranges from *4V* to *48V*.

At the axes of the hollow cathodes, the average electron temperature T_e falls as *ap* is increased with a minimum at approximately *8cm-torr*. The temperature of the slow electrons T_s varies little with *ap* though a slight peak is observed at *3cm-torr*. The fast electrons, however, manifest almost constant temperature T_f until *3cm-torr* before falling as *ap* is increased further. The temperatures at the side(*Figure*

Author(s) and Reference	Hollow cathode configuration†	Operating conditions	T_e and n_e‡	T_e and n_i‡	T_f and n_f‡
Howorka & Pahl [HOW72]	argon - ? *a=2.0cm* l_k*=7.4cm* Ratio l_k:*a=3.7* {2 anodes}	i_A : 5-20mA p : 0.1-0.5torr	T_e: 0.2-1.5eV falls with increasing i_A; gentler at high i_A (except 0.1torr which peaks at 10mA) n_e: (0.17-2.10)×10^{10}cm^{-3} increases almost linearly with i_A (except at 0.1torr; n_e constant up to 10mA before increasing with i_A)	T_i: 0.07-1.0eV decreases with increasing i_A n_i: (0.13-1.98)×10^{10}cm^{-3} increases linearly with i_A (except at 0.1torr; constant up to 10mA before increasing with i_A)	T_f: 2.0-3.2eV increases with i_A n_f: (0.03-0.19)×10^{10}cm^{-3} increases linearly with i_A
Tkachenko & Tyutyunnik [TKA76]	helium - nickel *a=3cm* l_k*=20cm* Ratio l_k:*a=6.7* {2 anodes}	i_A : 10-75mA p : 0.15-1.2torr	T_e: 0.5-6.0eV falls with increasing i_A; gentler at high i_A n_e: NOT AVAILABLE	T_i: NOT AVAILABLE n_i: NOT AVAILABLE	T_f: NOT AVAILABLE n_f: NOT AVAILABLE
Mizeraczyk [MIZ87]	helium - stainless steel *a=0.5cm* l_k*=0.77cm & 1.55cm* Ratio l_k:*a=1.54 and 3.10* {1 anode}	i_A : 2-50mA p : 5 & 10torr	T_e: 0.7-4.0eV falls steeply with increasing i_A up to ~(15-20)mA before increasing gently as i_A increases further n_e: (0.06-4.6)×10^{10}cm^{-3} increases linearly with i_A; smaller cathode diameter (p fixed) supports steeper gradient	T_i: NOT EVALUATED n_i: NOT EVALUATED	T_f: NOT EVALUATED n_f: NOT EVALUATED
present system	helium - stainless steel *a=0.65cm & 1.6cm* l_k*=1.2cm* Ratio l_k:*a=1.85*[1] *and 0.75*[2] {1 anode}	i_A : 5-40mA p : 1.5-15torr	T_e: 1.2-8.2eV falls with increasing i_A; gentler at high i_A (except at 1.5torr[1];minimum at 20mA after which increases with i_A steeply n_e: (0.8-77.6)×10^{10}cm^{-3} increases linearly with i_A (except at 9torr[1]; saturates at high i_A); smaller cathode diameter (p fixed) supports steeper gradient	T_i: 1.1-2.7eV decreases with increasing i_A (p=1.5[1],9[1&2]torr), increases with i_A up to 20mA; after which decreases(p=4.5torr[1]) or saturates(p=4.5torr[2]) n_i: (0.5-58.8)×10^{10}cm^{-3} increases linearly with i_A (except at 9torr[1];saturates after 20mA); smaller cathode diameter (p fixed) supports steeper gradient	T_f: 3.8-13eV increases with i_A (p=1.5[1],9[2]torr); increases with i_A up to 20mA before decreases(p=4.5[1&2],9[1]torr) n_f: (0.2-18.8)×10^{10}cm^{-3} - excludes p=1.5[1]torr for which n_f=43.2×10^{10} cm^{-3} at 40mA increases linearly with i_A except at 1.5torr[1] which shows non-linear increase and 9torr[1] which decreases with increasing i_A

(*Table 5.1.1*)

			SIDE	SIDE	SIDE
			T_e: 1.5-6.8eV falls with increasing i_A, gentler at high i_A (except at 1.5torr^1; increases with i_A up to 20mA before decreases & at 9torr^2 in which T_e increases with i_A n_e: (0.06-46) $\times 10^{10}$cm^{-3} increases linearly with i_A, smaller cathode diameter supports steeper gradient (p fixed)	T_s: 1.2-3.1eV decreases with increasing i_A in the HC6512; in the HC1612, decreases with increasing i_A up to 20mA before increases n_s: (0.9-43.8)$\times 10^{10}$cm^{-3} increases linearly with i_A; smaller cathode diameter supports steeper gradient (p fixed)	T_i: 4.4-17eV increses with i_A (except at 4.5torr^2 - decreases with increasing i_A up to 20mA before increases and at 15torr^1 of which T_i decreases with increasing i_A) n_i: (0.07-6.55)$\times 10^{10}$cm^{-3} increases linearly with i_A (except at 6torr^2 - increases with i_A up to 20mA before decreases)

† cylindrical hollow cathode; opened at both ends with the number of anodes as indicated
‡ parameters are measured at the axis of the hollow cathode unless otherwise stated
subscripts 1 HC6512
2 HC1612

Table 5.1.1 Comparing the behaviour of the plasma parameters (T_e, T_s, T_i, n_e, n_s and n_i) with respect to the discharge current i_A between reported works[HOW72, TKA76, MIZ87] and those obtained in the present system.

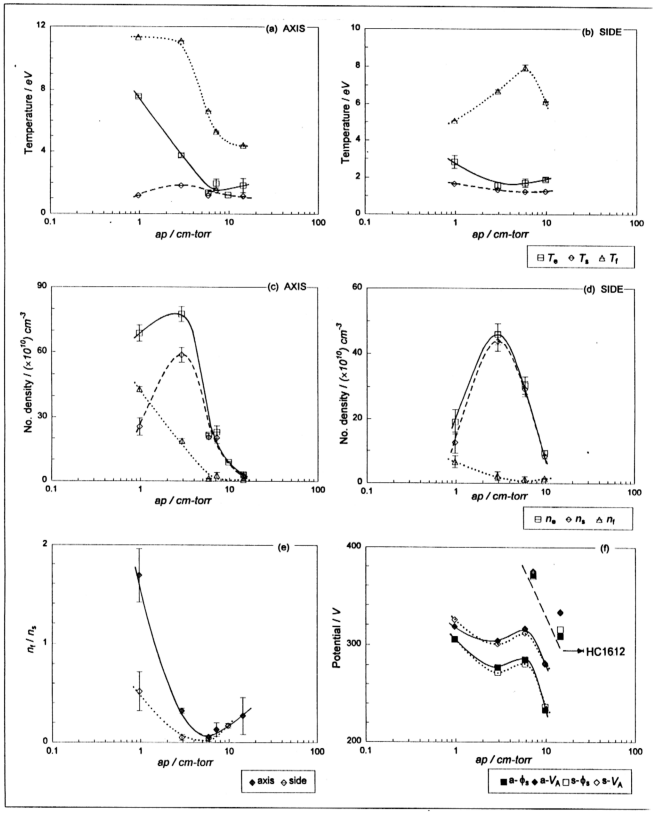

Figure 5.1.6 Variation of the plasma parameters (T_e, T_s, T_f, n_e, n_s, n_f, n_f/n_s, V_A and ϕ_S) deduced from the *log(I_e)* versus V_P plots with *ap* at two locations (axis[a] and side[s]) in the hollow cathode discharge operated at *40mA*.

5.1.6(b)) are shown only for the HC6512 as the side positions at both hollow cathodes are different. T_e and T_s here fall gently with increasing *ap* until approximately *(4-6)cm-torr*, after which they rise instead. On the other hand, T_f increases with *ap* until *6cm-torr* before decreasing with further increase of *ap*.

The total electron density n_e and the density of the slow electrons n_s rise with increasing *ap* until *3cm-torr*, after which they fall on further increase of *ap*. This behaviour is the same at the axis as well as the side of the hollow cathode. The density of the fast electrons n_f falls with increasing *ap*. The fall is rather steep (steeper at the axis) until approximately *6cm-torr*, after which it is almost constant at the axis but increases slightly at the side. The ratio of the number of fast electrons to the slow ones, n_f/n_s shown in *Figure 5.1.6(e)* falls with increasing *ap* until *6cm-torr* before rising slightly with further increase of *ap*. In relation to the *optimum pressure range*, it appears that the minimum n_f/n_s ratio corresponds to the upper limit of the range at *6cm-torr*.

For comparison purposes, the dependence of the plasma parameters on *ap* obtained from reported works by *Tkachenko and Tyutyunnik*[TKA76], *Howorka and Pahl*[HOR72] and *Mizeraczyk*[MIZ87] are plotted in *Figures 5.1.7(a)-(d)*, *5.1.8(a)-(d)* and *5.1.9(a)-(b)* respectively. The *optimum pressure range* is not clearly defined in the V_A–p plot of *Howorka and Pahl* but it is expected to occur at the region of inflexion. *Kirichenko, Tkachenko and Tyutyunnik*[KIR76] has shown that the position of the *optimum pressure range* is governed solely by the filling gas, independent of the cathode material. With *He* at *ap=(0.6-3)cm-torr*, the *optimum pressure range* in *Ar* was shown to shift to lower *ap* range of *(0.15-0.6)cm-torr*. Thus, the *optimum pressure range* of *Howorka and Pahl*(l_K:*a=3.7*) operated in Ar would be expected to

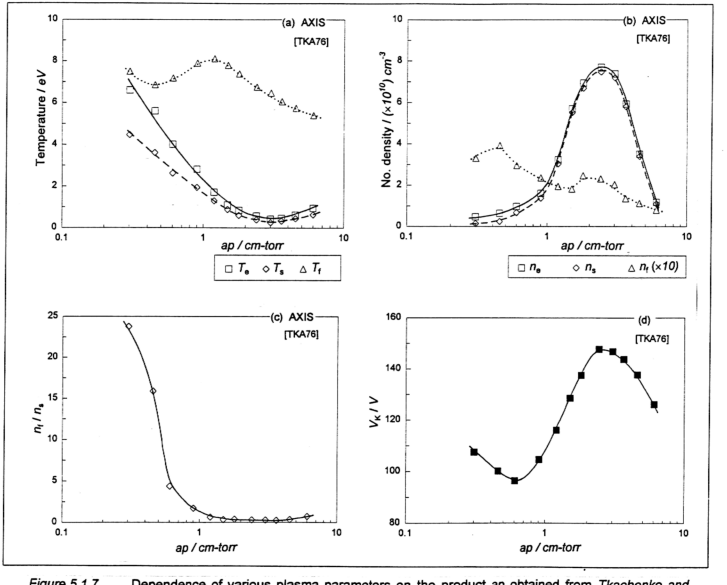

Figure 5.1.7 Dependence of various plasma parameters on the product *ap* obtained from *Tkachenko and Tyutyunnik*[TKA76].

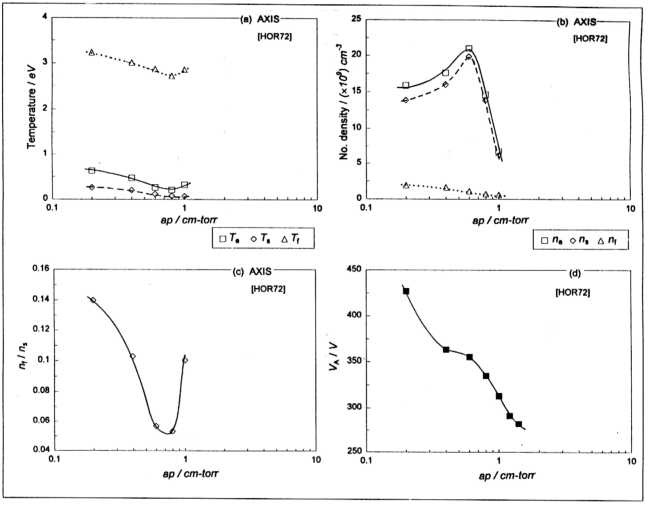

Figure 5.1.8 Dependence of the various plasma parameters on the product *ap* obtained from *Howorka and Pahl*[HOW72].

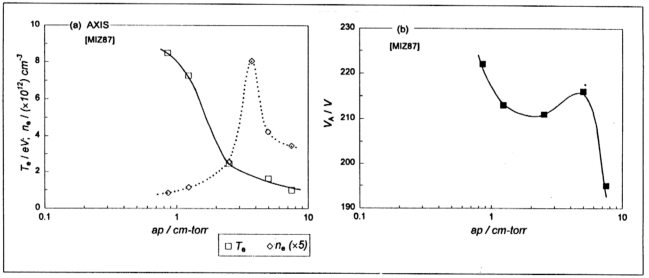

Figure 5.1.9 Dependence of T_e, n_e and V_A on the product *ap* obtained from *Mizeraczyk*[MIZ87].

occur in the thereabouts of *ap=0.5cm-torr* which is at the inflexion point, as the same range in a comparable system in *He* gas (HC1248 with l_K:*a=4* at *20mA*) occurs at approximately *(0.5-5)cm-torr*. The dependences of T_e and T_s on *ap* shown by the various authors and that obtained from the present system(at the axis and side) are similar, their respective minima occurring at slightly beyond or at the edge of the upper limit of the *optimum pressure range*. On the other hand, the trend of T_s with *ap* differs among the respective results. The trends of n_e, n_s and n_f with *ap* are similar from the various plots; though maxima exhibited by n_e and n_s from *Howorka & Pahl* and *Tkachenko & Tyutyunnik* correspond to the upper limit of the *optimum pressure range* while those from *Mizeraczyk* and present system occur at slightly before the same limit. This discrepancy could be related to the homogeneity of the hollow cathode discharge as the configuration of *Howorka & Pahl* and *Tkachenko & Tyutyunnik* have two anodes, one at each opened end of the cathode while the others have only one anode at one end. On the other hand, the ratios n_f/n_s show similar trends but with the minima occurring at slightly beyond the upper limits in the cases of *Howorka & Pahl* and *Tkachenko & Tyutyunnik* while that in the present system corresponds. A summary of the respective behaviour of the plasma parameters with *ap* from the various workers and the present system is given in *Table 5.1.2*.

The radial homogeneity of the hollow cathode discharge is checked by comparing the electron temperature and its density at the axis of the hollow cathode to those at the side (*2mm* and *4mm* off-axes for the HC6512 and HC1612 respectively). The ratio $T_{e\text{-AXIS}}$:$T_{e\text{-SIDE}}$ is given in *Table 5.1.3* while the square root of the ratio $n_{e\text{-AXIS}}$:$n_{e\text{-SIDE}}$ is plotted against i_A in *Figure 5.1.10*; a ratio larger than unity indicates that T_e (or n_e) is larger at the axis of the hollow cathode. The values

Author(s) and Reference	Hollow cathode configuration†	Discharge current and optimum pressure range	T_e, T_s and T_f‡	n_e, n_s and n_f‡	Ratio n_f/n_s
Howorka & Pahl [HOW72]	argon - ? *a=2.0cm* l_k*=7.4cm* Ratio l_k*:a=3.7* {2 anodes}	I_A : 20mA *ap* : <0.4-0.6>cm-torr¶	T_e, T_s, T_f: decreases with increasing *ap* exhibiting minimum at 0.8cm-torr before increasing slightly	n_e & n_s: increases with *ap* exhibiting maximum at 0.6cm-torr before decreasing n_f: decreases with increasing *ap*	decreases with increasing *ap* exhibiting minimum at 0.8cm-torr, after which increases
Tkachenko & Tyutyunnik [TKA76]	helium - nickel *a=3cm* l_k*=20cm* Ratio l_k*:a=6.7* {2 anodes}	I_A : 50mA *ap* : (0.6-2.4)cm-torr	T_e & T_s: decreases with increasing *ap* exhibiting minimum at 3cm-torr before increasing slightly T_f: decreases slightly until 0.43cm-torr, then increases until 1.2cm-torr, finally decreases with increasing *ap*	n_e & n_s: increases with *ap* exhibiting maximum at 2.4cm-torr before decreasing n_f: generally decreases with increasing *ap* though two peaks occur at 0.45 & 1.8cm-torr	decreases with increasing *ap* exhibiting minimum at 3.6 cm-torr, after which increases slightly
Mizeraczyk [MIZ87]	helium - stainless steel *a=0.5cm* l_k*=3.11cm* Ratio l_k*:a=6.22* {1 anode}	I_A : 50mA *ap* : (2-5)cm-torr	T_e: decreases with increasing *ap* T_s & T_f: NOT EVALUATED	n_e: increases with *ap* exhibiting maximum at 4cm-torr before decreasing n_s & n_f: NOT EVALUATED	NOT APPLICABLE
present system	helium - stainless steel *a=0.65cm & 1.6cm* l_k*=1.2cm* Ratio l_k*:a=1.85(HC6512) and 0.75(HC1612)* {1 anode}	I_A : 40mA *ap* : (2-6)cm-torr for the HC6512	T_e: decreases with increasing *ap* exhibiting minimum at ~8cm-torr before increasing slightly T_s: increases slightly exhibiting maximum at 3cm-torr before decreasing T_f: constant until 3cm-torr after which decreases with increase in *ap* SIDE T_e & T_s: decrease with increasing *ap* until ~(4-6)cm-torr, after which increases slightly T_f: increases with *ap* exhibiting maximum at 6cm-torr before decreasing	n_e & n_s: increses with *ap*, exhibiting maximum at 3cm-torr before decreasing n_f: decreases rather steeply with increasing *ap* until ~6cm-torr, after which almost constant SIDE n_e & n_s: increases with*ap* exhibiting maximum at 3cm-torr before decreasing n_f: decreases rather steeply with increasing *ap* until 6cm-torr, after which increases slightly	decreases with increasing *ap*, exhibitng minimum at 6cm-torr, after which increases SIDE decreases with increasing *ap*, exhibitng minimum at 6cm-torr before increasing

† cylindrical hollow cathode; opened at both ends with the number of anodes as indicated.
‡ parameters are measured at the axis of the hollow cathode unless otherwise stated.
¶ expected to be within the range though it is not clearly defined from the V_A against *p* plot.

Table 5.1.2 Comparing the behaviour of the plasma parameters (T_e, T_s, T_f, n_e, n_s, n_f and n_f/n_s) with respect to the product of the pressure and the hollow cathode diameter *ap* (and the optimum pressure range) between reported works[HOW72, TKA76, MIZ87] and those obtained in the present system.

of T_e and n_e here are averaged over the two methods of deduction, that is, from the $ln(I_e)$-V_p plots and the second derivative d^2I_e/dV_p^2-V plots. It can be noted from *Table 5.1.3* that T_e at the axis is generally higher than that at the side especially at low pressures (*2* and *6mbar*) and small hollow cathode diameter (an exception is observed for HC6512 at *2mbar*, *20mA*). At *12mbar*(HC6512), T_e at both positions are comparable. At *20mbar*(HC6512) and in the case of HC1612*(6* and *12mbar)*, T_e at the side is generally higher (within experimental error limit). These shall be compared to those deduced from the intensity ratio method to be discussed in *Section 5.2.3*.

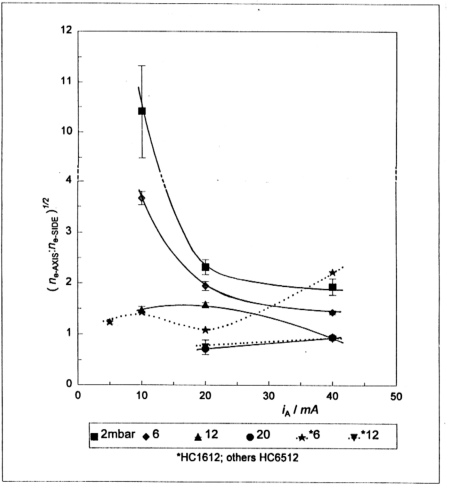

Figure 5.1.10 The radial homogeneity at various discharge currents i_A is checked by plotting the square root of the ratio $n_{e\text{-AXIS}}/n_{e\text{-SIDE}}$ against i_A.

		Ratio of $T_{e\text{-AXIS}}$: $T_{e\text{-SIDE}}$			
	p / mbar	*5mA*	*10mA*	*20mA*	*40mA*
HC6512	2		1.5±0.2	0.6±0.1	2.8±0.3
	6		1.3±0.1	2.1±0.3	1.8±0.2
	12		1.0±0.1	0.9±0.1	0.9±0.1
	20			0.8±0.1	0.8±0.1
HC1612	6	0.8±0.1	0.7±0.1	0.8±0.1	0.8±0.1
	12			1.4±0.5	0.8±0.1

Table 5.1.3 Table showing the values of the ratio of T_e measured at the axis to that at the side.

From *Figure 5.1.10*, it is deduced that the hollow cathode glow column grows radially as the discharge current i_A is increased especially at *2* and *6mbar* for the HC6512. This is evident from the very large number of electrons existing at the axis of the hollow cathode at low i_A in comparison to the side position; and their ratio decreases (eventhough the number densities at both positions increase (*Figure 5.1.2(c)-(d)*) upon increasing i_A. The observation of the radial intensity profile in *Section 5.2.1* supports this deduction. In the cases of HC6512 at *20mbar* and HC1612 at *12mbar*, the electron density n_e is higher at the side - this is also mirrorred in the radial intensity profile. Their number density ratio $n_{e\text{-AXIS}}$:$n_{e\text{-SIDE}}$ increases with i_A and it is, likewise observed for HC1612 at *6mbar*. This behaviour seems to be a feature of an annular hollow cathode glow column.

From the observations of the ratios $n_{e\text{-AXIS}}$:$n_{e\text{-SIDE}}$ and $T_{e\text{-AXIS}}$:$T_{e\text{-SIDE}}$ being close to unity (referring to *Figure 5.1.10* and *Table 5.1.3)*, it is then deduced that reasonable radial homogeneity is achieved only at large currents and high pressures. This is similar to the deduction of *Mizeraczyk*[MIZ87] on the axial homogeneity

which was shown to be attained in shorter hollow cathode lengths, larger currents and higher pressures.

5.1.2 The electron energy distribution function

The electron energy distribution function can be represented by the plot of the product of the second derivative of the electron current and the square root of the electron energy $d^2I_e/dV_p^2 \cdot V^{1/2}$ against the electron energy V. They are shown in *Figures 5.1.11* and *5.1.12* for fixed discharge current i_A and pressure p respectively. At fixed i_A=*40mA*, the peak of the electron energy distribution function increases in height as the pressure p is increased, the highest peak occurs at *12mbar*(HC6512) or *ap=5.85cm-torr*(close to the upper limit of the *optimum pressure range* depicted in *Figure 5.1.6(f)*), after which it decreases as p is increased further. At fixed p, the peak is higher for the smaller diameter. These behaviour are true at both the axis and the side of the hollow cathode. The peak of the electron energy distribution function is also observed to shift to lower electron energy as p is increased until *12mbar*(HC6512); beyond which it shifts to higher electron energy instead. At *2mbar*(HC6512), it can be seen from *Figure 5.1.11* that the electrons at higher energy is comparatively larger in number than those at other conditions; this is consistent with the ratio of n_f/n_s having value larger than unity determined from the $ln(I_e)$-V_p plots as shown in *Figure 5.1.3(a)*. At fixed pressure *12mbar*(HC6512), the peak of the electron energy distribution function grows in height on increasing the discharge current i_A at both the positions measured (see *Figure 5.1.12*).

Comparison of the electron energy distribution functions at the axes and sides of the HC6512 and HC1612 at fixed discharge current i_A=*40mA* is shown in

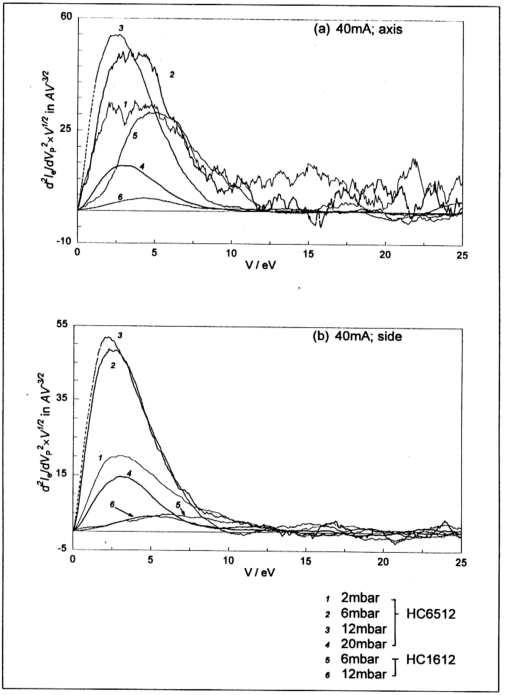

Figure 5.1.11 Variation of the electron energy distribution function (measured at the axis and side) with pressure p at fixed discharge current *40mA*.

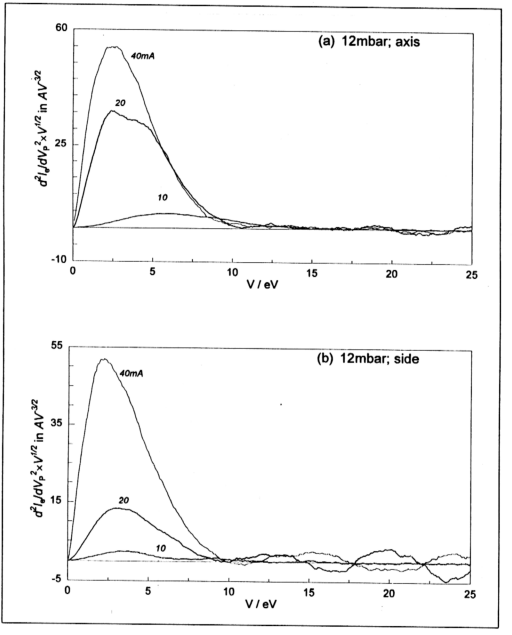

Figure 5.1.12 Variation of the electron energy distribution function with the discharge current i_A at fixed pressure *12mbar* at the axis and side of the HC6512.

Figure 5.1.13. It is observed that within the *optimum pressure range* of the HC6512 (*p=4-12mbar* or *ap=2-6cm-torr*), the electron energy distribution functions at both locations are comparable in shape and height eventhough the electrons at energies beyond the peak is slightly lesser in number at the side of the hollow cathode as the peak is slightly narrower. To the left of the *optimum pressure range*, the electron energy distribution function at the axis manifests much higher number of electrons within the range of electron energy studied (up to *25eV*) than at the side (*Figure 5.1.13(a)*). To the right of the optimum range, both the electron energy distribution functions are comparable again with the one at the axis showing slightly lesser number of electrons at energies beyond the peak instead (*Figure 5.1.13(d)*). In the HC1612, the peak of the electron energy distribution function at *6mbar* is much higher at the axis than the side. At *12mbar*, they are comparable though the electron energy distribution at the side shows higher number of electrons with energies larger than that at the peak - this is similar to those to the right of the *optimum pressure range* in the HC6512.

In order to check the type of distribution function, the experimentally obtained electron energy distribution function is normalized and compared to:

(a) the normalized Maxwellian distribution computed with T_e determined from the linear regions in the $ln(I_e)$–V_p plot in *Section 5.1.1*, and

(b) the normalized Druyvesteynian distributions computed with T_e and the average electron energy $\bar{V}$, both of which are determined from the integration of the d^2I_e/dV_p^2–V plots.

These are shown in *Figures 5.1.14(a)-(h)* for *p=2, 6, 12 & 20mbar* at fixed discharge current *40mA* in the HC6512 and in *Figures 5.1.15(a)-(d)* for *p=6 &*

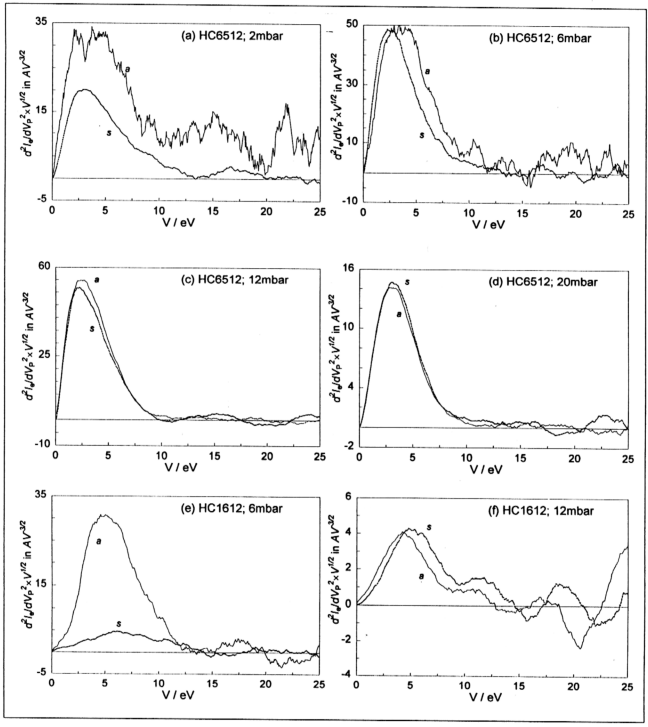

Figure 5.1.13 Comparing the electron energy distribution functions at the axis[a] and the side[s] for HC6512 and HC1612 at fixed discharge current i_A=*40mA* but different pressures *p* as indicated.

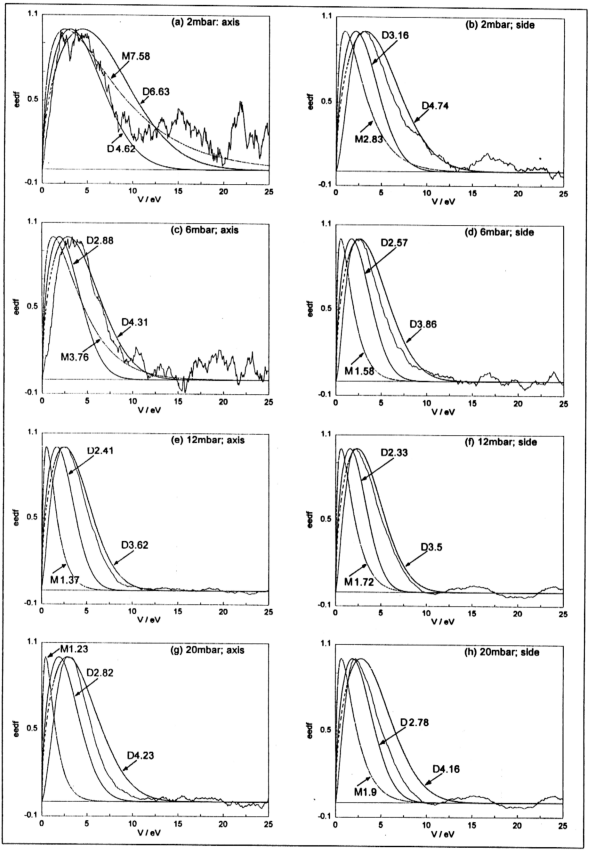

Figure 5.1.14 Comparing the normalized electron energy distribution functions in the HC6512 at fixed discharge current *40mA* to the computed Maxwellian[M] and Druyvesteynian[D] distributions.

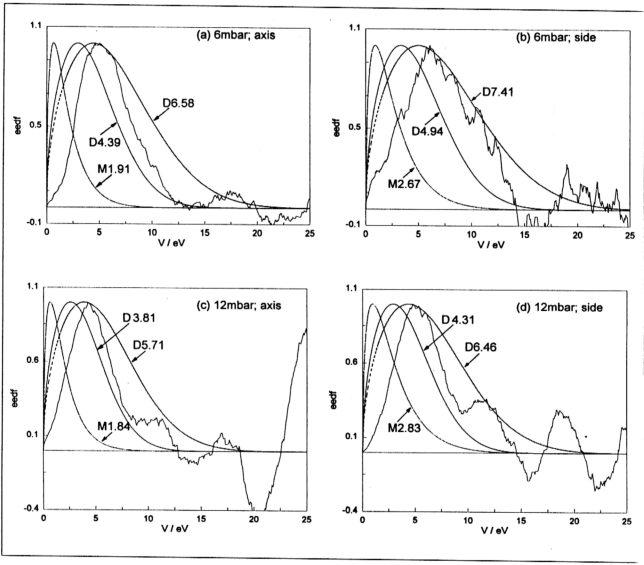

Figure 5.1.15 Comparing the normalized electron energy distribution functions in the HC1612 at fixed discharge current *40mA* to the computed Maxwellian[M] and Druyvesteynian[D] distributions.

12mbar at *40mA* in HC1612, inclusive of both locations in the hollow cathode. In the case of the functions obtained in HC6512, the electron energy distribution function at the axis agrees reasonably to a Maxwellian fit at low *p*(*2mbar* in *Figure 5.1.14(a)*). As *p* is increased, the function deviates from Maxwellian and tends to resemble a Druyvesteynian distribution computed with $\cdot\bar{V}$ until *12mbar*(at both the axis and the side of the hollow cathode). At *20mbar*, it also resembles a Druyvesteynian distribution but closer to the one computed with $T_e(=2\cdot\bar{V}/3$ in $eV)$. However, the measured function shows slightly narrower peak than the computed Druyvesteynian ones. In the case of HC1612, the electron energy distribution functions do not fit the Maxwellian nor Druyvesteynian types. The measured peaks here are much narrower than those manifested by the Druyvesteynian distribution computed at $\cdot\bar{V}$ though their peaks may coincide. The especially slow rise of the measured electron energy distribution function in the HC1612 at the low electron energy may not be true. This could be due to the shortcomings of the small plane probe itself - the knee at the between the electron retardation and saturation regions is not sharp. Furthermore, the electron saturation portion exhibits a curvature which is due an ill-defined charge collection region of the probe owing to edge effects[CHE65b].

In spite of the discussion above, it has been shown in *Section 5.1.1* that linear portions(due to Maxwellian-type distribution) on electron retardation region of the $ln(I_e)$–V_P could still be obtained. These linear slopes usually occur within the range of *(10-20)V* below the plasma potential. On closer examination of the electron energy distribution functions (measured and computed for Maxwellian), the slope of their falling edges do seem to match. Anyhow, the trend of the variation of the

plasma parameters with i_A and p discussed previously is similar irrespective of the whether they are deduced from the $ln(I_e)-V_P$ plots or integrated from the d^2I_e/dV_P^2-V plots eventhough their magnitudes may differ. Comparing with published works, *Tkachenko & Tyutyunnik*[TKA76] has also shown that the distribution is approximately Maxwellian in nature only at low $p(0.4mbar)$ in a *He-Ni* hollow cathode discharge (*3cm* diameter; *20cm* length; l_K:a=*6.7*). At $p>0.4mbar$, the measured electron energy distribution function was termed as 'mechanically deformed' Maxwellian. *Borodin & Kagan*[BOR66] also demonstrated Maxwellian electron energy distribution function only at low $p(=0.7mbar)$ in a *He* hollow cathode discharge (*2cm* diameter; *10cm* length; l_K:a=*5*) and deviations from the Maxwellian distribution are again obtained at higher pressures which exhibits excess of fast electrons. In both the cases, it was not confirmed if those distributions which deviated from Maxwellian belong to the Druyvesteynian type or not. In a transverse-type hollow cathode discharge[MIZ83] (*0.6cm* diameter; *6cm* length; anode embedded within the hollow cathode), it was shown that the electron energy distribution function was neither Maxwellian nor Druyvesteynian instead.

Most of the fast electrons capable of exciting and ionizing in the *He* discharge belong to the energy range of *(19-26)eV*, being responsible for most of the *HeI* emission lines observed (*Section 5.2.1*). In order to compare the contribution of this group of fast electrons to the radial spread of the emission profile when the pressure p is increased to be shown in *Section 5.2.1*, the ratio of the number of electrons within this energy range at the side(*2mm* off-axis in the HC6512) to that at the axis is estimated. The estimated ratios are *0.0208*, *0.0910* and *3.754* at p = *2*, *6* and *20mbar* respectively in the HC6512. The ratios for $p=12mbar$(HC6512) and for

the HC1612 are not estimated as their measured electron energy distribution functions tend to oscillate at the electron energy larger than *10eV*. These oscillations originate from the probe current signals and are exaggerated upon double differentiation of the probe characteristics. The increase of this ratio with pressure p is mirrorred in the radial spread of the *HeI 587.56nm* emission line profile shown in *Figure 5.2.6(b)*.

5.2 Spectral emission from the hollow cathode discharge

The choice of the width of the photodiode array (1024 channels) window and grating allows a spectral bandwidth of approximately *100nm* at every captured scan. Hence, five scans are required in order to obtain a visible spectrum ranging from *350nm* to *750nm*; each with the grating rotated such that the central position on the photodiode array is set for wavelengths *400, 475, 550, 625* and *700nm*. A sample of the spectrum obtained at the axis of HC6512 operated at *6mbar, 40mA* and *318-324V* in *He* gas is shown in *Figure 5.2.1*. The wavelengths(in *nm*) of the *He* lines observed in the present hollow cathode discharge are listed in *Table 5.2.1*. The appearance and the intensity of each line depend on the discharge conditions and hollow cathode configuration. Other lines observed include the hydrogen *656.28nm* and *486.13nm* possibly due to the water vapour present(*<3ppm*) in the *He* gas used. Though there is considerable sputtering in the hollow cathode discharge as evident from the observed deposition on the glass window at one end of the hollow cathode, no spectral line resulting from the elemental constituents of the cathode material is detected within the visible spectrum scanned.

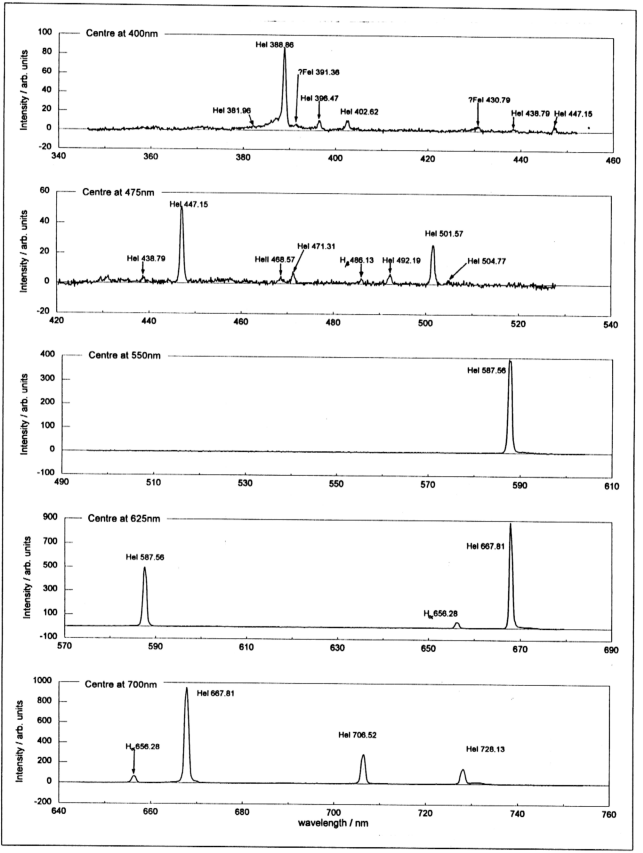

Figure 5.2.1 A sample spectrum detected at the axis of the HC6512 at *6mbar* and *40mA*.

a. Helium I

Triplet-triplet transition						Singlet-singlet transition					
$nd^3D - 2p^3P$		$ns^3S - 2p^3P$		$np^3P - 2s^3S$		$nd^1D - 2p^1P$		$ns^1S - 2p^1P$		$np^1P - 2s^1S$	
3d	587.56	*3s*	706.52	*3p*	388.86	*3d*	667.81	*3s*	728.13	*3p*	501.57
4d	447.15	*4s*	471.31			*4d*	492.19	*4s*	504.77	*4p*	396.47
5d	402.62					*5d*	438.79				
6d	381.96										

b. Helium II

$nf^2F^0 - 3d^2D$	
4f	468.57

Table 5.2.1 Wavelengths (in *nm*) of the *He* lines identified from the spectrum observed in the hollow cathode discharge.

5.2.1 Radial intensity distribution in the hollow cathode discharge

Parameters which have influence in the radial profile of the glow intensity of a hollow cathode discharge include the discharge current i_A, pressure p and the hollow cathode configuration. Different emission lines also exhibit their individual radial profiles. *Figures 5.2.2* and *5.2.3* show how the radial profile vary with i_A and p for one of the stronger intensity spectral lines detected at *667.81nm* in the HC6512 and HC1612 configurations respectively. The intensity of the radial profile increases with the discharge current i_A. At the low pressure range, the profile shows a maximum at the axis reminiscent of a bright central column of the negative glow. As the pressure is increased, this column becomes annular in shape as evident from the profile which shows a dip at the axis with two maxima, one each at the left- and right-hand glow edges. These maxima at the glow edges seem to move outwards as

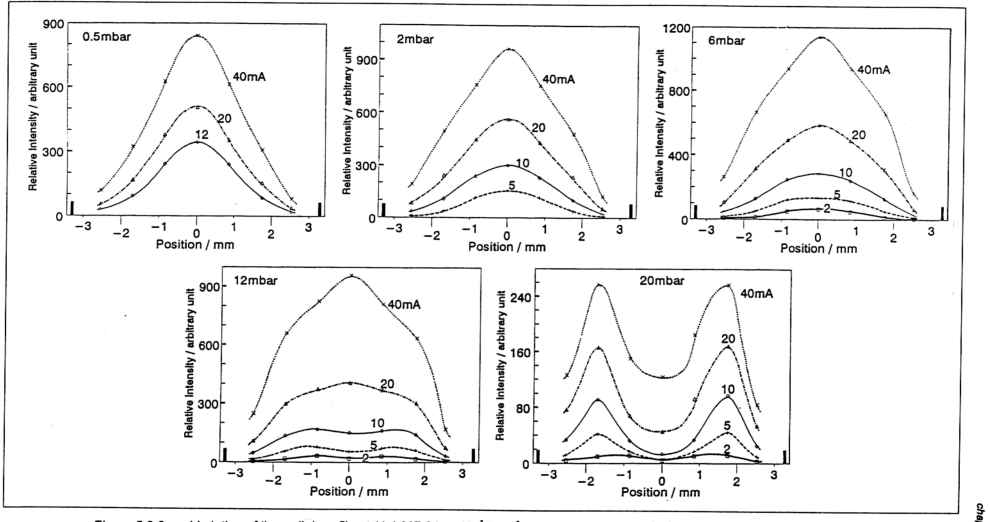

Figure 5.2.2 Variation of the radial profile at *HeI 667.81nm* ($3d^1D–2p^1P$) with the discharge current and pressure in the HC6512.

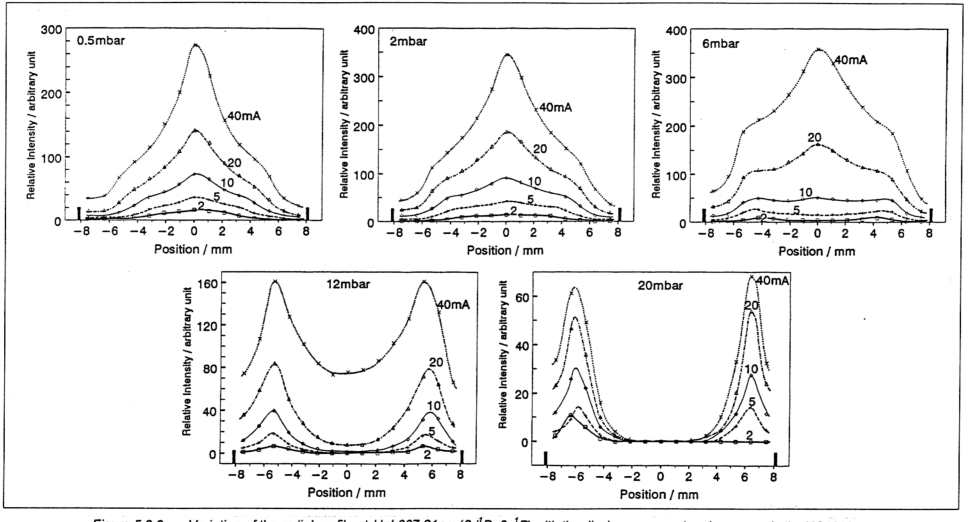

Figure 5.2.3 Variation of the radial profile at *HeI 667.81nm* ($3d^1D–2p^1P$) with the discharge current and pressure in the HC1612.

the pressure is further increased. On closer examination of the radial profiles, those which exhibit a central maximum tend to hint on the presence of two maxima at the left- and right-hand glow edges; being more distinct in the HC1612 configuration when compared to the HC6512. The ratio of the intensity of the maximum at the axis $I_{MAX\text{-}AXIS}$ to the average intensity of the maxima at the glow edges $I_{MAX\text{-}EDGE}$ in HC6512 and HC1612 are shown as a function of the pressure p for various fixed discharge current i_A in *Figures 5.2.4(a)-(b)*. A ratio greater than unity represents a full central cylindrical column of glow which is indicative of a coalesed negative glow defined for the hollow cathode effect. As the ratio dips below unity, the coalesed negative glow breaks up and the hollow cathode effect diminishes to that of a conventional planar cathode discharge. This transitional point occurs at $p=10mbar$ for $i_A=10mA$ in the HC6512 and at $p=2.5mbar$ for $i_A=2mA$ in the HC1612, moving to higher pressures when the current is increased. This behaviour is in agreement with the deductions drawn (as regard to the upper limit of the *optimum pressure range* shown in *Figure 4.2.5*) from the *V-p*(*i* fixed) curves in *Section 4.2.1.*

Among the transitions from possible excitation states in the singly ionized *He* atom, only *HeII 468.57nm* ($4f^2F^0$ - $3d^2D$) is detected in HC6512 and its radial profile is shown in *Figure 5.2.5.* The profile shows peak intensity at the axis and at times, two edge-maxima(of lower intensity levels) are also observed. However, these shapes may not be accurate as the overall intensity level is very low with poor resolution. The operating conditions of the hollow cathode discharge in which the *HeII 468.57nm* spectral line is discernable are at $i_A=40mA$ for $p=0.5\text{-}12mbar$ and at $i_A=20mA$ for a comparatively smaller pressure range of $p=6\text{-}12mbar$. In the hollow

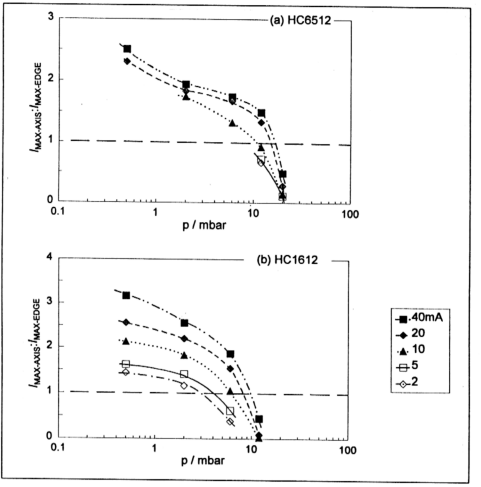

Figure 5.2.4 The ratio of the intensity of the maximum at the axis to those at the glow edge $I_{MAX-AXIS}:I_{MAX-EDGE}$ (deduced from the *HeI 667.81nm* radial profiles) plotted as a function of the pressure at various fixed discharge currents for (a) HC6512 and (b) HC1612.

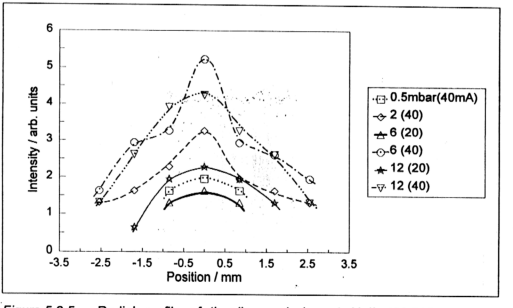

Figure 5.2.5 Radial profile of the line emission at *HeII 486.515nm* in the HC6512.

cathode of larger diameter HC1612, it was discernable only with a narrow central column profile at *40mA, 6mbar*. The range of the operating conditions under which this emission line from the ionized state of *He* atom is detected corresponds approximately to those of a fully developed hollow cathode discharge; and the smaller diameter hollow cathode HC6512 being more favourable than HC1612. The profile shape may be taken as an image of the concentration of the electron density of the very fast electrons toward the axis out of simple geometric reasons. The excitation functions of the atomic *HeI* lines generally peak at about *(30-40)eV*[KIE69] - this means that an electron which may attain the full cathode fall potential of *(200-400)eV* can excite many atoms one after the other. In contrast, the excitation function of this ionic *HeII* line becomes appreciable at electron energies larger than *75eV* and peaks at around *200eV*[KIE69] so that only unscattered electrons which have never undergone any collisions are able to excite these states. Initially these very fast electrons are directed toward the axis by the radial field in the cathode dark space. If they can keep this direction by not being scattered and then hit an atom, they could ionize and excite at the same time. The excited ions have short lifetimes and radiate immediately, their emission profile being a true picture of the density distribution of the exciting electron species[KUE81]. *Kuen et al*[KUE81] have shown similar profile of the ionic *HeII* lines(*468.5nm* and *320.3nm*) with a peak at the axis in a *He* hollow cathode discharge (*2cm* diameter; *4cm* length; l_K:*a=2*) at *2.3mbar* and *(10-25)mA*. The accumulation of the very fast electrons at the axis is also evident from the numerical calculation of the distribution function of the electrons with the Monte Carlo method by *Hashiguchi and Hasikuni*[HAS88] in a cylindrical hollow cathode of *1cm* diameter and *3.6cm* length at cathode fall potential of *300V*.

They also showed that the peak at the axis decreases with increasing gas pressure and these very fast electrons could hardly penetrate into the axis at $p=13mbar$. It can thus be inferred that the fully developed hollow cathode discharge can sustain electrons of energy as high as the cathode fall potential.

The behaviour of the radial profiles of different emission lines with their respective excitation functions could also indicate indirectly the connection between the electron energy distribution and radial co-ordinates. The lines chosen are *HeI 501.57nm*, *HeI 587.56nm* and H_α *656.28nm*. The transitions for the *He* lines were given in *Table 5.2.1* while the H_α line is from level *3* to *2*. The corresponding excitation functions are taken from *Reference* [KIE69]. The *HeI 501.57nm* originates from a singlet level, at about *23eV*, whose excitation function becomes appreciable at higher energies showing a peak at approximately *100eV*. The *HeI 587.56nm* originates from a triplet state, also at about *23eV*, but with an excitation peak at very little more. On the other hand, the H_α *656.28nm* originates from a lower energy of about *12eV*, exhibiting a sharp peak at a little more. Thus the *He* line intensity should indicate the presence of appreciable number of fast electrons, the hydrogen line those of comparatively lower energy. Unfortunately, none of the detected emission lines could be related to the low energy range. The radial profiles of the three emission lines in the HC6512 and HC1612 are shown in *Figures 5.2.6(a)-(c)* and *Figures 5.2.7(a)-(c)* for various pressures but fixed discharge current of *40mA*. All the profiles shown are normalized to their respective maxima. It could be observed that the maximum at the axis disappears at *20mbar* in the HC6512 and *12mbar* in the HC1612. In its place, two maxima are obtained on the left and right side of the axis. Considering only those profiles with the maximum intensity at the

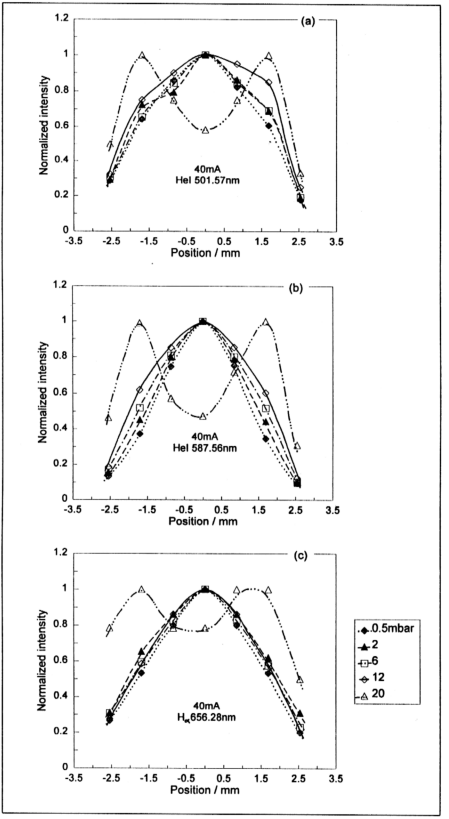

Figure 5.2.6 Normalized radial profiles of *HeI 501.57nm*, *HeI 587.56nm* and H_α *656.28nm* lines in relation to the pressure (i_A fixed at *40mA*) in the HC6512.

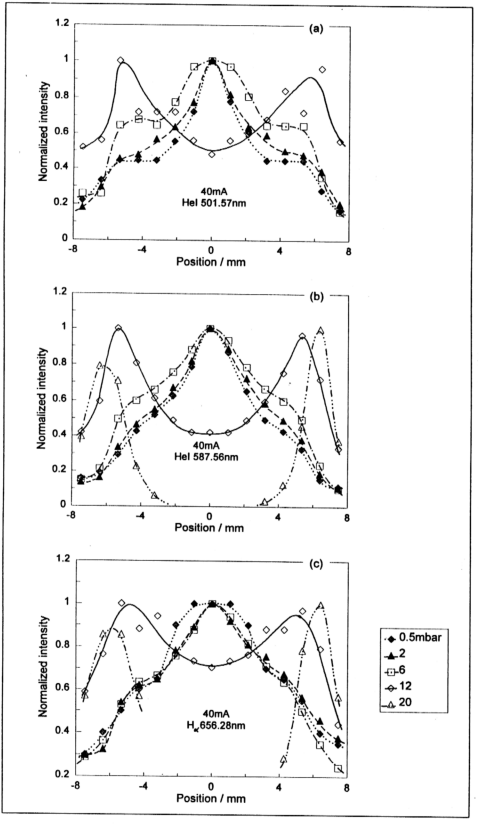

Figure 5.2.7 Normalized radial profiles of *HeI 501.57nm*, *HeI 587.56nm* and H_α *656.28nm* lines in relation to the pressure (i_A fixed at *40mA*) in the HC1612.

axis(as in a hollow cathode discharge condition), the spread of the profiles outwards with increase in pressure p is more pronounced for the *He* emission lines. The widest spread is at *12mbar* for the HC6512 and *6mbar* in the HC1612 which correspond approximately to the upper limit of their respective *optimum pressure ranges*. For the H_α *656.28nm* emission line, there is little radial spread of the profile with pressure in both hollow cathodes. This could indirectly indicate that the radial distribution of the number of electrons at a little more than *12eV* changes very little within the pressure range of *0.5mbar* to *12mbar*. In contrast, relatively more and more electrons at energies of around *23eV* and *100eV* move radially outwards as the pressure is increased.

5.2.2 Total intensity of the emission lines from the glow in the hollow cathode discharge

The total intensity of the line emission from the glow in the hollow cathode discharge is estimated by integrating over the total cross-sectional area of the hollow cathode as described in *Section 2.3*. *Figure 5.2.8(a)* shows how the estimated total intensities of the stronger emission lines in *HeI* vary with the discharge current at fixed pressure of *6mbar* in the HC6512. These include the singlet-singlet transitions *501.57nm* ($3^1P \rightarrow 2^1S$), *667.81nm* ($3^1D \rightarrow 2^1P$) and *728.13nm* ($3^1S \rightarrow 2^1P$); and the triplet-triplet transitions *388.86nm* ($3^3P \rightarrow 2^3S$), *447.15nm* ($4^3D \rightarrow 2^3P$), *587.56nm* ($3^3D \rightarrow 2^3P$) and *706.52nm* ($3^3S \rightarrow 2^3P$). *HeII 468.57nm* emission line is also included for comparison but it will have to be borne that the value of the slope is questionable as it is drawn from only two data points. It can be seen that the total intensities of the line emission in the *HeI* spectrum are $\propto i_A^{(0.8\text{-}1.2)}$ while that of the *HeII* spectrum

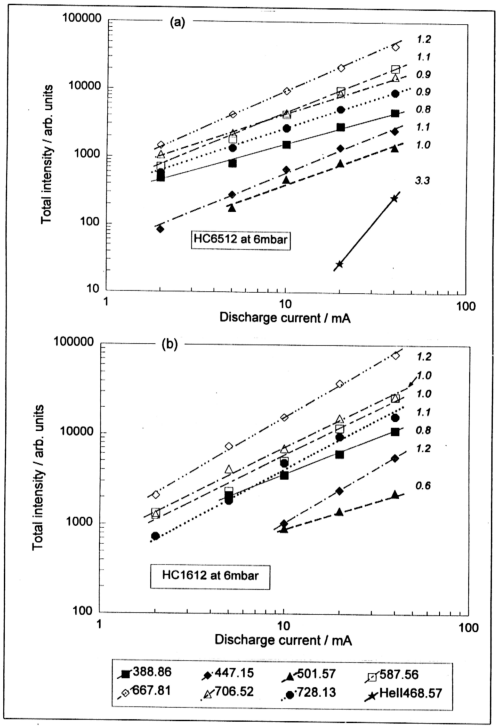

Figure 5.2.8 Relationship between the estimated total intensities of various emission lines and the discharge current at fixed pressure *6mbar* in (a) HC6512 and (b) HC1612.

is $\propto i_A^{3.3}$. In the case of HC1612, the total intensities of the *HeI* spectrum under the same conditions are $\propto i_A^{(0.6\text{-}1.2)}$ (see *Figure 5.2.8(b)*) while no slope could be deduced for the *HeII 468.5nm* line. The almost proportional dependence the intensities of the *He* lines to the discharge current is similar to those of the *Ne* lines shown by *Musha*[MUS62] in a *Ne-Mo* hollow cathode discharge (parallel plates of $4\times4cm^2$; *0.4cm* separation; l_K:*a=10*; *p=8mbar*). It was further shown that the intensities of the emission lines of *Mo* atoms vary nearly proportional to i_A^3. He then obtained the total radiation from the hollow cathode discharge to vary proportional to i_A^3 when compared to that from a conventional glow discharge which vary proportional to i_A only, and deduced that the hollow cathode discharge is dominated by the metal vapour of the cathode material and related this to the presence of negative resistance in the *V-i* characteristics. Unfortunately, the emission lines from the cathode material in the present setup are not detected.

Figure 5.2.9 shows the variation of the value of the slope of the logarithmic plot of the total intensity against the discharge current with the gas pressure *p* for the HC6512. The emission lines considered here belong to the transitions between the nearest level(see the first line in *Table 5.2.1*) in *HeI*. The slope value increases rapidly with *p* initially and slows down after *.2mbar*. It reaches a maximum at *12mbar* before dropping as *p* is increased further. Relating this to the *optimum pressure range*, it can be deduced that the hollow cathode discharge encourages the total intensity to increase the fastest with the discharge current when the hollow cathode effect is fully developed.

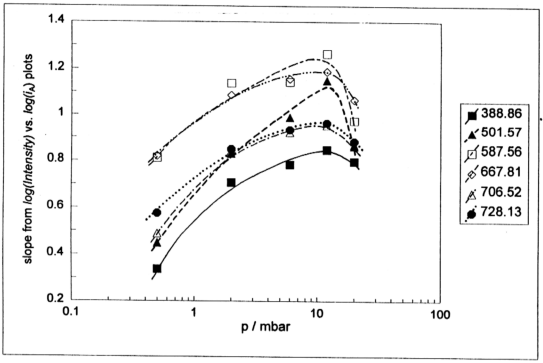

Figure 5.2.9 Variation of the slope of the logarithmic plot of the total intensity against the discharge current i_A with the gas pressure p in the HC6512.

On the variation of the total intensity of the stronger emission lines with the pressure, it could generally be observed that they increase slowly with pressure p until $\approx$*12mbar* in HC6512 and $\approx$*6mbar* in HC1612, after which they decrease quite rapidly with further increase in p. These are shown in *Figures 5.2.10(a)-(b)*. Though the total intensity values are evaluated until *12mbar* for the *HeII 468.57nm* line, its total intensity level could be observed to increase more rapidly with pressure initially when compared to the *HeI* lines before exhibiting a peak between *6mbar* and *12mbar*. Again, the occurrence of the turning point here may roughly be related to the upper limit of the *optimum pressure range*.

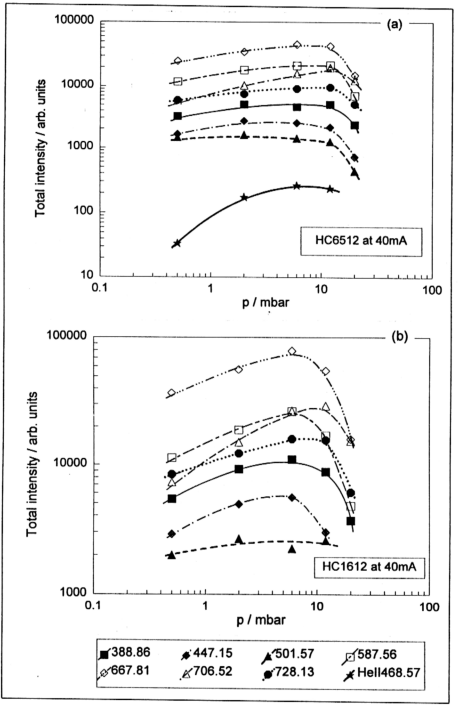

Figure 5.2.10 Variation of the total intensity of the stronger emission lines with pressure at fixed discharge current *40mA* for (a) HC6512 and (b) HC1612.

5.2.3 Radial temperature profile in the hollow cathode discharge

With reference to *Section 3.4.1* as to the requirements and assumptions of the different models to be used in the deduction of the electron temperature from the line intensities, the simplest and most direct method is to adopt the local thermodynamic equilibrium model. The temperature of the plasma in the hollow cathode discharge is then determined from the relative intensities of a pair of emission lines of the same atomic specie. Among the detected lines in the *HeI* spectrum, approximately ten pairs of spectral lines can be evaluated. Though accuracy can be improved by taking a large number of pairs of different lines or to take a combination pair with larger energy difference, only two pairs involving four spectral lines of sufficiently strong intensity can be relied on to give reasonably accurate results. These combination pairs are the singlet-singlet transitions of $728.13nm(3^1S \rightarrow 2^1P)$: $667.81nm(3^1D \rightarrow 2^1P)$ with energy difference of *0.154eV* and the triplet-triplet transitions of $706.53nm(3^3S \rightarrow 2^3P)$:$587.57nm(3^3D \rightarrow 2^3P)$ with energy difference of *0.355eV*.

The variation of the estimated electron temperature T_e profiles with pressure p at fixed discharge current *40mA* are shown in *Figures 5.2.11(a)* and *(b)* for the HC6512 and HC1612 respectively. These electron temperatures shown are deduced as weighted averages of the two temperatures estimated from the two combination pairs of spectral lines mentioned above. The T_e profiles in the HC6512 tend to be bell-like shaped except for the *20mbar* though all of them show a maximum at the axis. Whereas in the HC1612, three maxima (the highest one at the axis while the other two lower ones are at the left-hand and right-hand side of the axis) are observed in the T_e profiles for p=*0.5*, *2* and *6mbar*. At *12mbar*, the three maxima are

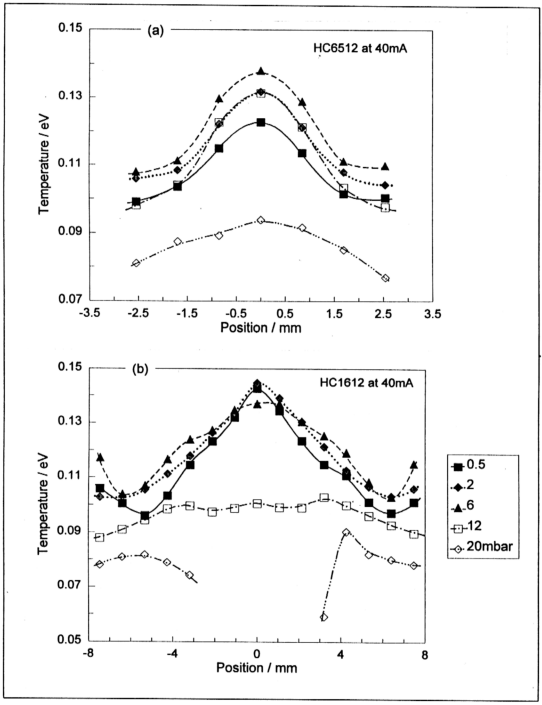

Figure 5.2.11 The electron temperature (estimated from the line intensities ratio method) profiles at *40mA* and various *p* in the (a)HC6512 and (b) HC1612.

comparable in height. The T_e profile at *20mbar*(HC1612) is not complete due to the intensity levels at the vicinity of the axis being too low to allow any sensible estimation of the temperature. The relationship between the T_e (at the axis and side of the hollow cathode discharge) and the product of the hollow cathode diameter and the pressure *ap* is shown in *Figure 5.2.12*. The T_e at the side is estimated at *2mm* off-axis for the HC6512 and *4mm* for the HC1612 in order to make comparison with those obtained through the Langmuir probe method shown in *Figures 5.1.6(a)-(b)*. At the axes of HC6512 and HC1612, T_e increases initially from ≈*0.3cm-torr* until ≈*3cm-torr* before falling with increasing *ap* while those measured via the probe decreases with increasing *ap* from ≈*1cm-torr* until ≈*8cm-torr* before increasing slightly. On the relation of T_e at the side with *ap*, T_e increases with *ap* initially until ≈*3cm-torr* for HC6512 and ≈*8cm-torr* for HC1612 before falling as *ap* is increased further. This behaviour is again different from that shown in *Figure 5.1.6(b)* where T_e at the side(HC6512) decreases initially with increasing *ap* until ≈*4cm-torr* before increasing slowly as *ap* is further increased.

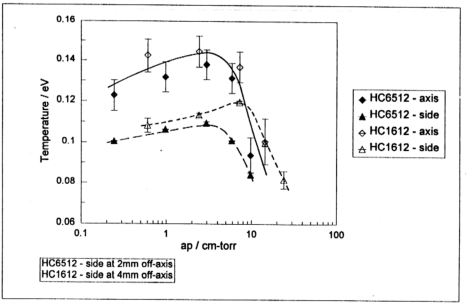

Figure 5.2.12 Variation of T_e estimated from the line intensity ratio method with the product *ap* for HC6512 and HC1612 at i_A=*40mA* monitored at the axis and the side.

The variation of the estimated electron temperature T_e(at the axis and side) with discharge current i_A at fixed pressure p are shown in *Figures 5.2.13(a)-(b)* for the HC6512 and in *Figures 5.2.13(c)-(d)* for the HC1612. It can be seen that T_e is generally higher for larger i_A and this is different from the behaviour observed using the probe technique (see *Figure 5.1.2(a)-(b)*).

From the above discussions, quite a number of discrepancies between the behaviour of the T_e estimated from the relative line intensity ratio method and the Langmuir probe diagnostic method are realised. Furthermore, the absolute magnitude of the electron temperature T_e estimated here are approximately one order of magnitude lower than those deduced from the probe diagnostic method in *Section 5.1.1*. As discussed in *Section 3.4.1*, these discrepancies could be due to the electron densities(measured with the Langmuir probe) which are at least four orders of magnitude lower than those valid in the assumed local thermodynamic equilibrium. Another violation involves the assumption of Maxwellian distribution while most of the actual electron energy distribution functions measured are of the Druyvesteynian type (except at low p) as discussed in *Section 5.1.2*. Though the radial intensity distribution is measured at the imaged cross-sectional plane of the hollow cathode discharge, it is likely that the assumption of a homogeneous plasma column is not satisfied. The glow within the hollow cathode could be observed to grow outwards axially especially at low p and high i_A and the thickness of the glow column within hollow cathode would not be uniform. It has already been shown by *Kirichenko et al.*[KIR76] that the penetration depth of the discharge in the hollow cathode depends on the pressure p and current i_A. This problem could have been corrected by Abel's tranform but for the unknown thickness or penetration depth of

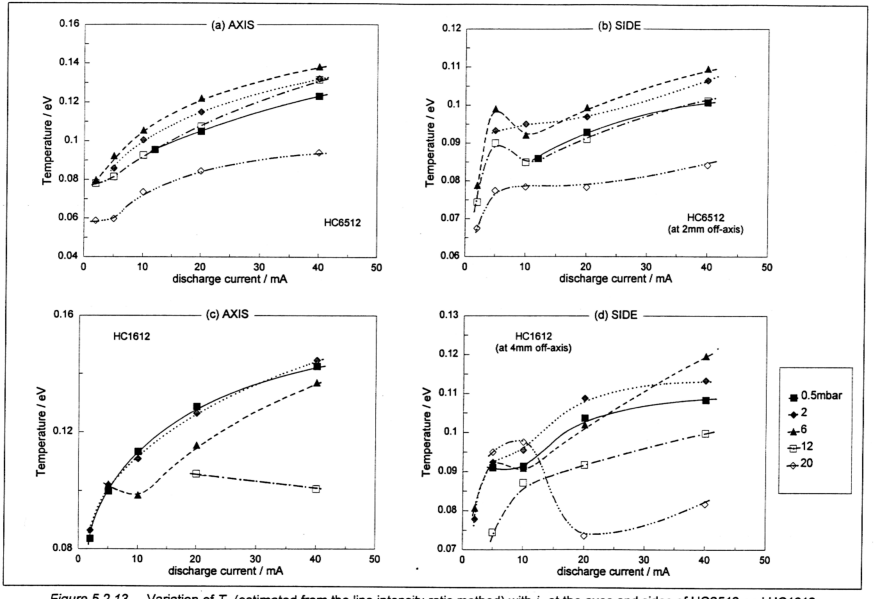

Figure 5.2.13 Variation of T_e (estimated from the line intensity ratio method) with i_d at the axes and sides of HC6512 and HC1612.

the glow column at each line intensity detection point.

Furthermore, errors incurred in the estimation of the temperature are unavoidable. The relevant atomic transition probabilities used in the temperature calculation taken from reference [WIE66] are quoted to have uncertainties within *3%*. Other errors incurred include the correction factors for the spectral response of the photodiode array, the absorption of light in the glass window(which may be coated in some instances) as well as the non-uniformity of the intensity level measured at different channels in the photodiode array. All these contribute to an additional uncertainty of approximately *3%*. On top of all these, the digitized value of the intensity level is assumed to have an uncertainty of ± 1. This would introduce large error ($>100\%$) when the ratio of low intensity levels are used; especially at small currents and/or large pressure.

5.2.4 Cathode dark space width in the hollow cathode discharge

Various methods has been used to determine the cathode dark space width d_K. *Little & von Engel*[LIT54] defined it as the distance between the cathode to the point where the electric field is zero. Another way to define the edge of the dark space is to move the anode towards the cathode while keeping the current constant until the point where the voltage rises abruptly; however, this is only true for low values of V_K[FRA56]. The method adopted here makes use of the measured radial profile of the glow intensity as described by *Kirichenko et al*[KIR76]. The boundary between the negative glow and the cathode dark space is then defined as the point at which the gradient of the glow intensity is a maximum. However, it is not possible

to clearly defined a maximum gradient in the case of the HC6512 radial profile of the glow intensity due to the small number of points of detection across its diameter (seven points as compared to fifteen points in the HC1612) as well as the shape of its profile. It is then more appropriate to take the point at half its maximum intensity.

The cathode dark space width d_K as a function of the pressure p at various discharge currents i_A is determined from the radial profile of stronger intensity *HeI* lines at λ = *388.86, 447.15, 587.56, 667.81, 706.52 and 728.13nm* and is shown in *Figures 5.2.14(a)* and *(b)* for HC6512 and HC1612 respectively. The d_K values shown are averaged values over all the strong intensity lines. At low i_A, d_K decreases with increasing pressure p; being extremely steep in the hollow cathode of larger diameter HC1612. As i_A is increased at fixed p, d_K generally gets narrower (especially for p<*10mbar*). At high i_A and over the mid-pressure range, the cathode dark space width d_K is observed to remain almost constant. The occurrence of this constant width falls within the *optimum pressure range* as shown in the relevant V_A–$p(i_A$ fixed) curves of *Figures 5.2.15(a)-(b)*. Similar comparison has been reported by *Kirichenko et al*[KIR76] in a *He-Ni* hollow cathode discharge(*3cm* diameter; *20cm* length; l_K:*a=6.7*). It can thus be concluded that the width of the cathode dark space remains constant when the hollow cathode effect is fully developed in agreement to that which has been reported by *Little and von Engel*[LIT54].

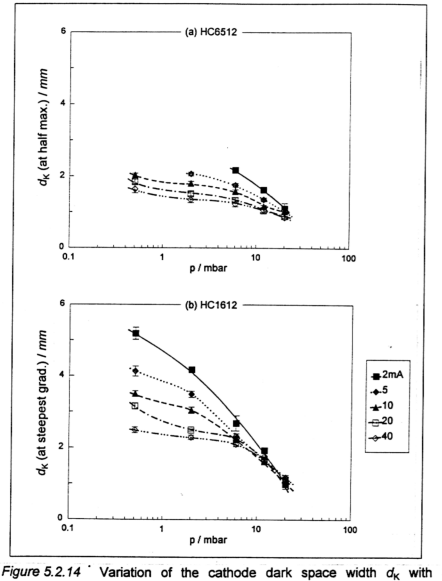

Figure 5.2.14 Variation of the cathode dark space width d_K with pressure p for (a) HC6512 and (b) HC1612

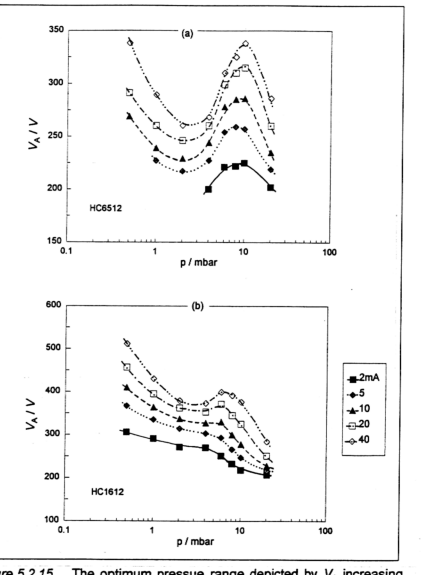

Figure 5.2.15 The optimum pressue range depicted by V_A increasing with p in the V-$p(i_A$ fixed) curves for (a) HC6512 and (b) HC1612

5.3 Sputtering of the hollow cathode material

During the acquisition of the radial distribution of intensity levels, the glass window at one end of the hollow cathode is found to be coated after the hollow cathode discharge has been sustained for some time (usually a few minutes). This coating is found to be most pronounced at low *He* pressure (*0.5mbar*) and high current (*40mA*) as judged by visual inspection of the layer of material deposited. It can also be deduced that the rate of deposition is dependent on the discharge current and the pressure; being low at low current and high pressure. This is because the sputtering rate is known to depend markedly on gas pressure and geometry of tube; being experimentally shown to be constant at low pressure but falls appreciably at higher pressure due to back diffusion of ejected atoms to cathode[FRA56]. This sputtering process is due to the ejection of particles of the cathode substance by impact of ions from the discharge; and its rate is dependent on the energy of the bombarding ion which, in turn, is proportional to the reduced electric field *E/p*. In the hollow cathode configuration, the electric field falls linearly from the cathode towards the edge of the coalesced negative glow where the field is near zero[LIT54,TAK86]. As most of the potential fall is across the cathode dark space, the average value of the electric field can be estimated from the ratio of the cathode fall potential V_K and the width of the dark space d_K(from *Figures 5.2.14(a) and (b)*); assuming that $V_K \approx (V_A - 25)V$ of which the difference is the averaged differences shown in *Figure 5.1.6(f)* and V_A is the sustaining voltage. In comparison, *Kirichenko et al*[KIR76] have shown that V_K and V_A differ by $\approx 20V$. It can be seen from *Figure 5.3.1* that the estimated value of *E/p* in the cathode dark space is higher at lower

pressure and higher current, thereby, resulting in the ions which traverse from the glow bombarding the cathode with higher attained energy. This leads to higher sputtering rate (resulting in more deposition) at low pressure and high current.

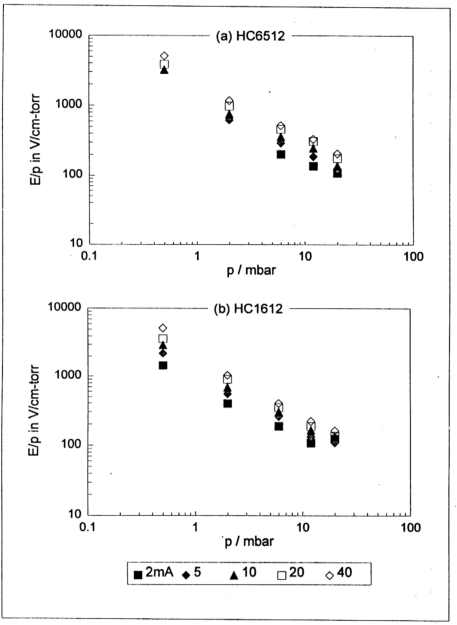

Figure 5.3.1 Logarithmic plot of the estimated reduced field *E/p* across the dark spaces in the HC6512 and HC1612 with $V_K=(V_A-25)V$ and d_K is obtained from *Figures 5.2.14(a) & (b)*.

Pictures of these coated surfaces are shown in *Figure 5.3.2*. The shiny and reflective surface (whitish in colour) observed is likely to result from the sputtering of metallic material from the *stainless steel* cathode. At high current where heating of the cathode is most pronounced, annular rings (yellowish and brownish in colour) are noticed. This is, however, possibly due to the deposition of the evaporated hydrocarbons from the fluoroelastomer 'O'-ring seal seated in between the cathode and the glass window. The shape of the coated surfaces is reminiscent of the radial profile of the glow intensity - filled rings are observed for low pressure and annular ring with hollow axis at high pressure.

The deposited metallic layer due to the sputtering of materials from the *stainless steel* cathode is confirmed by a qualitative analysis of the coating utilizing the *EDXA* (Energy-Dispersive X-ray Analysis) method in the *SEM* (Scanning Electron Microscope). The elemental constituents of the coated portion of the glass window identified from the *EDXA* spectrum given in *wt%* (average of three sets taken at different sites chosen at random) as compared to that of an unused clean glass window(average of only two sets) is given *in Table 5.3.1*.

Element	Na	Mg	Al	Si	K	Ca	Cr	Fe
Coated glass[a]	5.89	2.76	2.11	63.90	1.32	14.71	2.17	7.14
Unused clean glass[b]	9.30	4.21	2.12	68.65	1.81	13.15	0.43	0.68
Ratio of a:b	0.6	0.7	1.0	0.9	0.7	1.1	5.0	10.5

Table 5.3.1 Comparison between the elemental constituents identified from the *EDXA* spectrum for the coated glass window and the uncoated one. Values quoted in the 2nd and 3rd row are given in *wt%*.

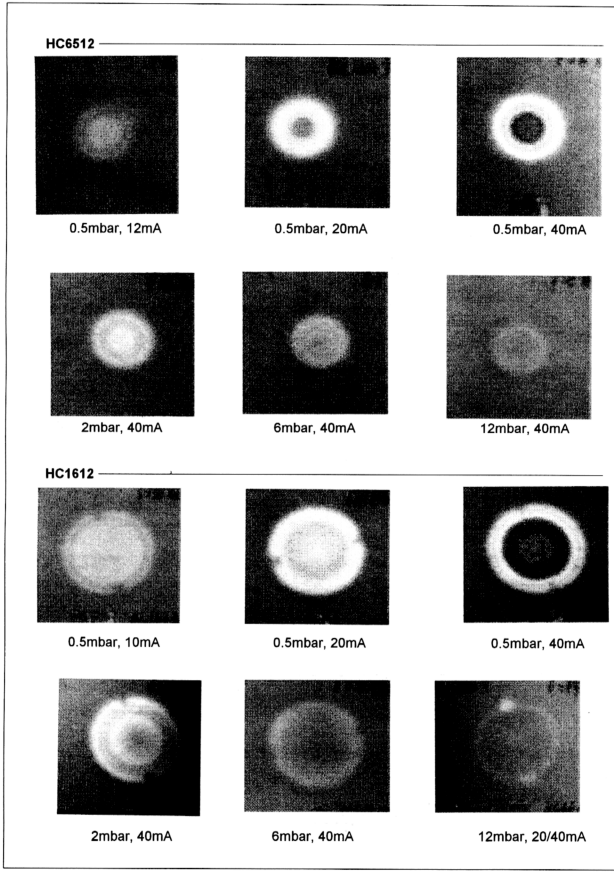

Figure 5.3.2 Visual impression of the patterns of the deposited coatings on the glass windows placed at one of the opened ends of the hollow cathodes HC6512 and HC1612 under the indicated operating conditions.

Significant differences in the elemental constituents of the coated and unused clean glass pieces are observed for *Cr* and *Fe* with ratio much larger than unity and these two elements are the major constituents present in most types of *stainless steel*. For example, *stainless steel* of type *Immaculate 5* is made up of *52.28%Fe + 24.0%Cr + 21.5%Ni + 1.3%Si + 0.8%Mn + 0.12%C*[TUR62].

He gas discharge is actually expected to give very low sputtering yield. This is because the sputtering rate by gas depends immensely on the relative masses of metal and gas atoms, that is, gas atoms of mass closely approximating to that of the metal atoms are the most efficient sputterers[PIL81]. It is thus believed that the sputtering yield from *He* gas discharges could be due to the presence of impurities. (For example, the tank of purified grade of *He* gas used contained *1vpm* of hydrocarbons, *<3vpm* of moisture and *<3vpm* of oxygen as stated by manufacturer. This also explains the relatively strong H_α *656.28nm* and H_β *486.13nm* spectral lines observed in the emission studies of the *He* hollow cathode discharge.)

The spatial non-uniformity of the coating as well as the different rate of deposition as a function of current and pressure will introduce error in the measured intensity levels in the radial profile measurement since each point is taken at different times, especially if comparison among the radial intensity distribution under various conditions is to be made. Steps taken to minimise these sources of inaccuracy include reducing the discharge current during the break in-between reading the intensity levels (when the spectrum is being stored in the hard disk) and while tuning the monochromator to change to the next range of spectrum to be measured; especially under high current and low pressure operation of the hollow cathode discharge and changing the glass window when necessary.